Title: Early Human Pulmonary Lesions Define a Permissive Alveolar Niche for *Mycobacterium tuberculosis*

Authors: Rosane M. B. Teles[1], Chaouki Benabdessalem[2], Jonathan Perrie[3], Cenfu Wei[4], Julie West[1], Bruno J. de Andrade Silva[1], Priscila R. Andrade[1], Lilah A. Mansky[1], Prajan Divakar[5], Linda Fischbacher[6], Karen Lam[1], Feiyang Ma[1], Yiqian Gu[3], Kimia Rategh[1], Aparna Pillai[1], Samuel M. French[7], Emna Romdhane[8], Mohamed-Ridha Barbouche[2]*, Eynav Klechevsky[9], Marco Colonna[9], Adrie J. C. Steyn[10], Steven J. Bensinger[11 12], Daniel L. Barber[13], Soumaya Rammeh[8], Parambir S. Dulai[4], Bryan D. Bryson[14], Matteo Pellegrini[3], John T. Belisle[6], Barry R. Bloom[15], and Robert L. Modlin[1 11]

Affiliations: [1]Division of Dermatology, Department of Medicine; [3]Department of Molecular, Cell, and Developmental Biology; [7]Department of Pathology; [11]Department of Microbiology, Immunology and Molecular Genetics; [12]Department of Molecular and Medical Pharmacology, David Geffen School of Medicine, University of California, Los Angeles, CA, USA. [2]Laboratory of Transmission, Control and Immunobiology of Infections, Institut Pasteur de Tunis, University of Tunis El Manar, Tunis, Tunisia. [4]Northwestern University, Chicago, IL, USA. [5]Bruker Spatial Biology, Bothell, WA, USA. [6]Department of Microbiology, Immunology and Pathology, Colorado State University, Fort Collins, CO, USA. [8]Department of Pathology, Charles Nicolle Hospital, Tunis, Tunisia; LR23ES02, Faculté de Médecine de Tunis, Université de Tunis El Manar, Tunis, Tunisia. [9]Department of Pathology & Immunology, Washington University in St. Louis, St. Louis, MO, USA. [10]Africa Health Research Institute, Durban, South Africa. [13]Laboratory of Parasitic Diseases, NIAID, NIH, Bethesda, MD, USA. [14]Massachusetts Institute of Technology, Cambridge, MA, USA. [15]Harvard T.H. Chan School of Public Health, Boston, MA, USA. *Current address: Department of Microbiology, Immunology and Infectious Diseases, College of Medicine and Medical Sciences, Arabian Gulf University, Manama, Bahrain.*

Corresponding author: *Robert L. Modlin, M.D. (email:rmodlin@mednet.ucla.edu)*

Abstract

Understanding mechanisms of pathogenesis and protection in human tuberculosis (TB) remain major global health challenges. While organized granulomas have long been the focus of TB research, growing evidence for asymptomatic transmission highlights the need to study earlier disease stages, particularly TB pneumonia, which remains underexplored. Defining the alveolar immune niche that governs bacillary expansion before granuloma formation is essential for interrupting transmission. Here, we integrate spatial transcriptomics, single cell RNA sequencing, and high resolution imaging of human lung biopsies to map early TB pneumonia and compare with adjacent granulomas within the same tissues. Pneumonic alveolar spaces were dominated by TREM2-associated macrophages, characterized by sparse T cell infiltration, minimal antimicrobial gene expression, and abundant *Mycobacterium tuberculosis* antigens and transcripts. In contrast, granuloma cores were enriched for antimicrobial pathways, were surrounded by multiple cell types that walled off infection, and contained comparatively fewer bacterial markers. Our findings identify TREM2 positive 'foamy' macrophages as a key permissive alveolar niche for *M. tuberculosis* survival and growth. These cells represent an attractive target for early intervention to restrict infection and limit transmission.

.

One Sentence Summary

Early TB pneumonia defines an alveolar niche that fosters bacterial persistence and transmission before granuloma formation.

Introduction

Tuberculosis (TB) remains a leading global cause of infectious mortality. A critical and under-recognized challenge is asymptomatic (subclinical) transmission: prevalence surveys indicate that roughly half of active cases in endemic settings are asymptomatic at the time of detection, yet harbor live *Mycobacterium tuberculosis* (*M.tb*) (*1*). Moreover, cough is not required for transmission, normal tidal breathing can account for ~90% of exhaled bacilli over 24 hours (*2*). These findings imply that early, minimally symptomatic pulmonary lesions can shed bacilli and drive epidemic spread (*1, 3*). Understanding the alveolar immune niche that enables bacillary growth prior to granuloma formation is therefore central to interrupting transmission.

Granulomas, organized structures of macrophages and lymphocytes, have long been considered the hallmark TB lesion (*4*). Yet since the 19th century, pathologists have observed that TB can begin as a bronchopneumonia (*5*). In most individuals, initial infection is controlled or latent (*6*). When containment fails (e.g., HIV co-infection (*7*), immunosuppressive therapy (*8*), TB often first presents as pneumonia with foamy, lipid-laden macrophages filling alveoli (*9*), only later evolving into granulomas with epithelioid macrophages, multinucleated giant cells, and lymphocytic mantles (*10, 11*).

Foamy macrophages within the alveolar pneumonia contain abundant cholesteryl esters and triglycerides (*9, 12*) and can serve as a nutrient-rich reservoir for *M.tb* (*13*). These early lesions typically show sparse T cell infiltration, contrasting with granulomas enriched in Th1, Th17, and cytotoxic T cells (*14-16*). We hypothesized that foamy macrophages create a permissive alveolar niche where bacilli expand unchecked, seeding subsequent pathology.

Across lipid-rich diseases, macrophages adopt a conserved TREM2^{+} lipid-associated program, characterized by TREM2 and lipid-handling genes such as *APOE* and *PLIN2* (*17-20*). TREM2 signaling promotes foamy macrophage formation and anti-inflammatory states (*21*). Prior work shows that mycobacterial lipids can also engage TREM2 (*22, 23*). Thus, we hypothesized that foamy macrophages in early TB pneumonia represent TREM2^{+} macrophages

establishing a permissive niche. Here, using spatial transcriptomics, scRNA-seq, and high-resolution imaging of human TB lung biopsies taken in early suspected disease, we define these lesions, map bacterial distribution, and test whether *M.tb* lipids and TREM2 pathways drive the foamy state. Our findings support a model where TREM2^{+} foamy macrophages serve as a key permissive alveolar niche for bacillary survival and transmission.

Results

We analyzed lung biopsies from patients with untreated pulmonary TB, each containing regions of acute pneumonia adjacent to organized granulomas (*10, 16*). Histologically, the pneumonia lesions were evident as clusters of alveoli filled with aggregates of foamy (lipid-rich) macrophages, replacing the normal airspaces (**Figure 1A-D**) (*16*). In contrast, nearby granulomas showed the expected architecture: dense central collections of epithelioid macrophages and multinucleated giant cells, often with central necrosis, surrounded by a mantle of lymphocytes (*16*). These two lesion types were often adjacent, underscoring that the foamy macrophage pneumonia represents an earlier stage within the same infected region of lung that can give rise to granulomas over time (*24*).

Using GeoMx spatial transcriptomic profiling, we quantitatively compared gene expression in microdissected regions of interest (ROIs) from alveolar pneumonia, granuloma cores, and granuloma mantles (**Figure 1E–H, Supplemental Table 1, Supplemental Figure 1**). Unsupervised clustering of the transcriptomes clearly segregated ROIs by their spatial location (alveoli vs. core vs. mantle), indicating distinct molecular signatures for each compartment (**Figure 1I, Supplemental Figure 2**). Differential expression analysis revealed that the alveolar (pneumonia) regions were enriched for genes involved in lipid metabolism and surfactant handling, consistent with the presence of foamy macrophages within the alveolar pneumonia and Type II pneumocytes. Notably, the alveoli showed high expression of mRNAs encoding apolipoproteins and lipid-processing enzymes (e.g. *APOE*, *APOC1*, *LIPA*), as well as scavenger receptors like *CD36* and *CD163* (**Supplemental Figure 3A, B**), which are known markers of alternatively activated, lipid-associated macrophages (*25, 26*). Alveolar regions also contained transcripts from alveolar type II epithelial cells (*SFTPA2, SFTPC* encoding surfactant proteins) (*25*), reflecting epithelial cells lining alveoli. In stark contrast, the granuloma core regions over-expressed a suite of pro-inflammatory and antimicrobial genes, including *IL1B, CYP27B1,* and *MT2A*, as well as *CYBB* (NOX2 subunit mediating reactive oxygen production)

(*26*) (**Supplemental Figure 3A, C**). These core signatures are indicative of classically activated ("M1-like") macrophages and Th1/Th17-type T cells working to control infection. The granuloma mantles were enriched for B and T lymphocyte genes (e.g. *IGHG, CD3E, CD8A*), consistent with lymphocyte clustering around granulomas(*27*) (**Supplemental Figure 3B, C**). By computing the set intersection of genes differentially expressed in one region versus the other two, we identified signature genes for each region: alveoli=559, core=414, and mantle=803 (**Supplemental Table 3**).

What are the cell types and their gene signatures that comprise human pulmonary TB?

We next used scRNA-seq on the lung tissue to identify specific cell populations present in these lesions. Clustering of ~45,000 cells yielded a total of 27 cell types, which were identified by comparing to the scRNA-seq cluster signatures to known cell signatures including major cell types (*28, 29*), a human lung atlas (*30*), leprosy lesions (*31*) and using Enrichr (**Figure 1J, Supplementary Table 4, Supplemental Figure 4A**). Notably, among five distinct macrophage clusters, we identified a cluster corresponding to "TREM2$^+$ lipid-associated macrophages" as well as "IFN-activated macrophages", "SPP1$^+$ macrophages", "interstitial macrophages", "alveolar macrophages". The T cell populations included: CD8$^+$ T cells, naïve (or resting) T cells, Th17 cells (with features of Th1 cells and MAITs), NK/T-CTL/ γδ T cells (reflecting cells with expression of genes in the cytotoxic pathways including NK cells, tri-cytolytic T cells (T-CTL) and γδ T cells), and Tregs. These populations were stable across the four different patients (**Supplementary Figure 4B**).

What are the differences in frequency of cell types between TB pneumonia and organized granulomas?

By comparing the scRNA-seq cluster signatures with the spatial transcriptome data, we could infer which cell types predominated in each region of the tissue. Strikingly, the alveolar

pneumonia regions showed the strongest overlap with the TREM2$^+$ macrophage gene signature (adjusted p value, $p < 10^{-10}$) (**Figure 1K**). In other words, the foamy alveolar ROIs were dominated by the TREM2$^+$ macrophage cluster, confirming that those lipid-loaded cells in the alveoli correspond to the TREM2-expressing, lipid-associated macrophages identified by scRNA-seq. Consistently, the alveolar regions also overlapped with signatures of "alveolar macrophages" and "interstitial macrophages", whereas the granuloma core overlapped most with "SPP1$^+$ macrophages" and IFN-activated macrophages. The location of "TREM2$^+$ macrophages" in the alveoli is consistent with the location of foamy macrophages in alveoli. The granuloma core contained "SPP1$^+$ macrophages", "IFN-activated macrophages" and "Th17 cells". The granuloma mantle zone contained "B cells", "plasma cells", "CD8$^+$ T cells" and "LAMP3$^+$ DC".

Overlap of the GeoMx spatial signature genes from each region with cell type markers from a scRNA-seq healthy lung atlas (*30*) confirmed the cell locations from the pulmonary TB scRNA-seq data, also revealing that the alveoli had a strong overlap with gene signatures from "AET1" and "AET2" (**Supplemental Figure 5A**). Overlap with our previous studies of leprosy lesion scRNA-seq data (*31*) confirmed that the alveoli had the strongest overlap with gene signatures from "TREM2$^+$ macrophages", consistent with the location of foamy macrophages in alveoli (**Supplemental Figure 5B**).

We further assessed the different host responses in the granuloma and pneumonia by functional pathway analysis of the pulmonary TB DGE signatures from the GeoMx spatial profiling data. The alveoli DGEs were enriched for lipid metabolism, localization and transport, typical for TREM2$^+$ macrophages, as well as surfactant metabolism (**Supplemental Figure 6A**). The core DGEs were enriched for innate immune responses including responses to bacterium while the mantle DGEs were enriched for T and B cell pathways, consistent with the histology of this region and the overlap with leprosy scRNA-seq marker sets. Similar analysis of the pulmonary TB scRNA-seq myeloid cell gene signatures indicated that IFN-activated

macrophages and SPP1$^+$ macrophages were enriched for “defense response to bacterium” and “antimicrobial humoral immune response mediated by antimicrobial peptide” (**Supplemental Figure 6B**). The TREM2$^+$ macrophage and alveolar macrophages were enriched in lipid metabolism pathways.

Do TREM2$^+$ macrophages preferentially localize to the alveoli in TB pneumonia?

To further clarify the location of TREM2$^+$ macrophages in pulmonary TB, we derived a gene signature using a consensus set of 34 TREM2$^+$macrophage related scRNA-seq gene signatures from 21 publications (**Supplemental Table 7**), ranking the frequency of genes in these signatures (**Supplemental Tables 8 and 9**). Overlap with the pulmonary TB DGEs revealed that the twelve most highly ranked TREM2 macrophage signature genes had a higher overlap with alveoli than core, with the ratio of the Jaccard indices greater than 5, for genes found in ≥22 signatures (**Supplementary Figure 8A, B**). The expression of eight genes, LGMN, CTSD, TREM2, NPC2, APOE, C1QB, GRN and C1QC was greater in the alveoli vs. core, whereas C1QA expression was almost equal and CTSB was greater in the core, with MS4A6E and FTL not detected in the GeoMx data (**Supplemental Figure 8C**). We examined the TREM2$^+$ macrophage scRNA-seq signature genes, which significantly overlapped with the gene expression in the alveoli in the GeoMx data ($q<10^{-10}$). Eleven of the twelve TREM2$^+$ macrophage genes listed above were indeed present in the TREM2$^+$ macrophage scRNA-seq cluster from our scRNA-seq data (all except MS4A6E).

Given that TREM2$^+$ macrophages are characterized by expression of lipid metabolism genes(*17*), we mined the TREM2$^+$ macrophage scRNA-seq data, finding enrichment for genes for lipid metabolism pathway genes characteristic of lipid localization, lipid metabolism, lipid signaling, response to lipids, cholesterol transport and cholesterol efflux (**Supplemental Figure 8D, Supplemental Table 10**). Of these, *TREM2*, *APOE*, *CTSD*, *NPC2*, *PLIN2*, *LIPA*, *PSAP*, *CD81*, *APOC1* and *HEXB* were present in 17 of the 34 TREM2$^+$ macrophage gene

signatures. Together, these data demonstrate that the TREM2^{+} macrophages expressing lipid metabolism genes are predominantly located in the alveoli of the pulmonary TB pneumonia.

Do antimicrobial programs differ between pneumonia and granulomas?

Spatial and single-cell analyses revealed striking compartmentalization of antimicrobial responses within the same lungs. Early TB pneumonia in alveoli was dominated by lipid-associated macrophages and showed minimal expression of canonical TB antimicrobial products, whereas organized granulomas exhibited a concentrated antimicrobial inflammatory profile. Using a curated panel of 52 antimicrobial genes from the Antimicrobial Peptide Database 3(*32*) and key mycobacterial host-defense genes (*31, 33*) (**Supplemental Table 5**), we detected markedly fewer antimicrobial transcripts in alveolar ROIs compared with granuloma cores (3/52 vs. 15/52, $q < 10^{-6}$), despite the bacterial burden in pneumonia. By region, eight antimicrobial genes were detected in granuloma cores (adj. $p = 6.78\times10^{-5}$), five in the mantle (ns), and three in alveoli (ns) (**Supplemental Figure 7A-B; Supplemental Table 6**). Direct comparison showed a significant enrichment of antimicrobial transcripts in granuloma cores relative to alveoli (15 genes, adj. $p = 3.72\times10^{-7}$).

Of the 52 antimicrobial genes, 40 were expressed across T cell and myeloid subsets in scRNA-seq of human pulmonary TB (**Supplemental Figure 7C-D; Figure 1L**). The granuloma cores showed the broadest antimicrobial profile: IFN-activated macrophages expressed 15 antimicrobial genes, SPP1^{+} macrophages eight, Th17 cells seven, and NK/T-CTL/γδ T cells four. In the mantle, CD8^{+} T cells expressed three antimicrobial genes, LAMP3^{+} dendritic cells six, and monocyte-like cells four. Notably, several of these encode proteins with direct antimycobacterial activity: *CAMP* (cathelicidin) in SPP1^{+} and alveolar macrophages (*34*); *GNLY* (granulysin) in CD8^{+} T and NK/T-CTL/γδ T cells (*31, 35, 36*); *IL26* in Th17 cells (*37*); and *S100A12* in monocytes (*38*). This dichotomy highlights the functional specialization of the

lesions: granulomas are immunologically organized for containment, whereas the early pneumonia is relatively permissive to *M. tb*.

What are the differences in the frequency of cell types as defined by specific protein determinants between and TB pneumonia and the organized granulomas?

We validated these findings at the protein level using high-resolution spatial proteomics (NanoString CosMx) and immunohistochemistry on serial tissue sections. Staining for macrophage and T cell markers recapitulated the lesion architecture: $CD68^+$ macrophages and Langhans giant cells concentrated in granuloma cores, $CD3^+$ T cells and $CD20^+$ B cells forming a mantle around granulomas (**Figure 2A, B**). The ratios and aggregation of T cells and B cells in the mantle zone varied among granulomas (**Supplemental Figure 9**). Strikingly, $CD163^+$ macrophages filled the alveolar spaces of the pneumonia (**Figure 2A, C**). CD163 is a scavenger receptor induced in M2-polarized and foamy macrophages, and its presence correlated with the foamy macrophages in alveoli. Within alveoli, macrophages varied in CD68/CD163 expression, either $CD163^+$-predominant (**Figure 2D**) or $CD68^+CD163^+$ co-expressing (**Figure 2E**), yet were uniformly foamy on H&E. In contrast, $CD3^+$ T cells were rarely present (**Figure 2F and Supplemental Figure 10**).

The $CD163^+$ foamy macrophages in alveoli were often found in close proximity to granulomas, for instance, surrounding small nascent granulomas or in alveoli adjacent to a granuloma mantle (**Supplemental Figure 9A, 11**). This spatial relationship supports the concept that some, if not most granulomas arise physically within, the broader foamy macrophage pneumonia. Another hallmark feature of pulmonary TB, bronchiole obstruction, a mechanism associated with spread of the infection (*11*), was visualized with surrounding lymphocytic infiltrate containing T and B cells, necrosis, and obliteration of the bronchiolar

epithelium such that the airway was occluded by necrotic granulomas (**Supplemental Figure 12**).

By standard immunohistology, we detected $CD3^+$ and $CD4^+$ lymphocytes throughout the granuloma, with $CD8^+$ and $CD20^+$ lymphocytes predominantly localized to the mantle zone (**Supplemental Figure 13A-D**). $CD68^+$ macrophages and Langhans giant cells were confirmed to be in the core of the granuloma, with CD163 identifying macrophages in alveoli (**Supplemental Figure 13E, F, and Supplemental Figure 14**).

What are the differences in localization and phenotype of $TREM2^+$ macrophages in the TB alveolar pneumonia compared to granulomas?

Immunostaining for TREM2 itself revealed a striking pattern: TREM2 protein was highly expressed on the foamy macrophages in the alveolar pneumonia, with strong membrane staining on those cells, whereas granuloma macrophages and giant cells had only weak or patchy TREM2 (**Figure 3A, Supplemental Figure 15 A-D**). We confirmed that the macrophages in the alveolar pneumonia co-expressed CD163 with TREM2 (**Figure 3A-B**). The macrophages in the alveoli expressed the lipid droplet marker perilipin-2 (PLIN2), CD68, APOE, LIPA and SPP1 (**Figure 3A, Supplemental Figure 15E**), indicating they contained abundant intracellular lipid droplets as shown by perilipin-2 (PLIN2) staining (a lipid droplet coat protein)(*39*). PLIN2 immunofluorescence exhibited a punctate pattern throughout the macrophages in the alveolar pneumonia, confirming their foamy, lipid-loaded nature (**inset of Figure 3A and Supplemental Figure 16A**). In sum, these data identify a population of $TREM2^+$, $CD163^+$, $PLIN2^+$ foamy macrophages specifically localized to TB alveolar pneumonia, distinct from the macrophages inside granulomas.

Staining for the major cell wall lipoglycan LAM and for purified protein derivative (PPD, a mix of mycobacterial proteins) revealed intense antigen signals in the macrophages within the alveolar pneumonia, whereas the cores of the granulomas showed little to no signal (**Figure 3A,**

C, D; Supplemental Figure 16B-C) (*40, 41*). Antigen deposits appeared granular and co-localized with foamy macrophages. By immunofluorescence, TREM2 co-localized with LAM in macrophages within the alveolar pneumonia (**Figure 3C**) (*42*), indicating that the very TREM2$^+$ foamy macrophages are the cells harboring mycobacterial lipid antigens. Moreover, PLIN2$^+$ lipid droplets were often adjacent to or overlapping with LAM signals (**Supplemental Figure 16D**), consistent with the known interaction of bacilli and bacterial lipids with host lipid stores(*9, 13*).

Do TREM2$^+$ foamy macrophages in TB pneumonia harbor *M.tb* mRNAs, indicating bacterial persistence?

A critical question was whether foamy macrophages within the alveolar pneumonia serve as the main bacterial reservoir in TB pneumonia. Acid-fast microscopy often detects few bacilli in patient biopsies (*13*), raising the possibility that organisms persist in non-replicating or masked states. To address this, we employed in situ hybridization for *M.tb* mRNAs.

RNAscope for multiple *M.tb* transcripts (e.g., esxA, fbpB/85B) revealed clusters of mRNA signals within macrophages in the alveolar pneumonia, even in areas where acid-fast staining was negative (**Figure 3E; Supplemental Figure 14**) (*43*). These transcript clusters likely correspond to intracellular bacterial groups. By contrast, in organized granulomas we observed only sparse *M.tb* mRNA puncta, typically as single dots in a few macrophages. Thus, the highest bacterial burden resided in the foamy macrophages in the alveolar pneumonia, not in cores of the granulomas. Taken together, the antigen staining and RNA hybridization provide compelling evidence that TREM2$^+$ foamy macrophages in the alveolar pneumonia represent the primary host cell reservoir for *M.tb* in the lungs of pulmonary TB patients.

What is the role of TREM2$^+$ macrophages in TB pathogenesis?

Having established the presence of TREM2$^+$ foamy macrophages in TB pneumonia, we next asked how TREM2 expression is induced on these cells and whether it is functionally

activated. TREM2 is a receptor that senses lipids and apoptotic debris (*44-46*). Two classes of signals were considered: (i) host cytokines, since IL-4/IL-13 drive alternative macrophage activation and upregulate TREM2 (*47, 48*), and (ii) *M.tb* cell-envelope lipids. In vitro, we confirmed that IL-4 treatment increased TREM2 expression on ~30% of monocyte-derived macrophages, consistent with prior studies (*47*). We then tested two major *M.tb* lipids: phthiocerol dimycocerosate (PDIM) and free mycolic acids. Both potently induced TREM2 surface expression (~50-55% of cells), a level surpassing even live *M.tb* infection (~30% at MOI 5-10) **(Figure 4A and Supplemental Figure 17A)**. By contrast, lipoarabinomannan (LAM) and peptidoglycan failed to induce significant TREM2.

We next assessed whether these lipids also activated TREM2 signaling. Using a fluorescent TREM2–DAP12 reporter, which clusters upon ITAM–SYK pathway engagement (*23*), we found that both PDIM and free mycolic acids robustly triggered intracellular TREM2–DAP12 activation, with a strong correlation between surface TREM2 induction and signaling activity ($r = 0.93$, $p = 0.007$) (**Figure 4A and Supplemental Figure 17B)**. In contrast, LAM and peptidoglycan produced no significant reporter activation. These results establish that *M.tb* lipids not only induce TREM2 expression but also directly stimulate its signaling cascade.

Given our finding that TREM2$^+$ macrophages in TB pneumonia contained PLIN2$^+$ lipid droplets, we next asked whether the same *M.tb* ligands that induced TREM2 in vitro could also drive lipid storage. Infection of macrophages with *M.tb* is known to trigger lipid droplet biogenesis (*13*), a process linked to host immunometabolic reprogramming (*49*). Consistent with this, treatment of human MDMs with either of the two virulence lipids, free mycolic acids or PDIM, as well as with IL-4, produced a two-fold increase in lipid droplet accumulation relative to untreated controls (**Figure 4B, Supplemental Figure 18A**). Moreover, direct infection of TREM2$^+$ macrophages with *M.tb* resulted in ~50% greater lipid droplet formation compared to uninfected TREM2$^+$ counterparts (**Figure 4C, D**). While mycolic acids were previously shown to

induce lipid droplets(*13*), our data newly identify PDIM, a recognized virulence determinant (*24, 41, 50-52*), as a potent driver of this foamy macrophage phenotype.

Do TREM2$^+$ macrophages support or restrict *Mb* growth?

We considered why foamy, TREM2$^+$ containing macrophages would favor the bacteria? One hypothesis is that excess lipid droplets and associated metabolic changes might impair bactericidal functions of macrophages while providing nutrients for *M.tb*. We observed in tissue that TREM2$^+$ foamy macrophages co-localized with abundant *M.tb* antigens and mRNAs, whereas more classically activated macrophages in granulomas did not. To directly test the functional relationship between the foamy macrophage phenotype and *M.tb* viability, we conducted infection experiments in vitro.

Human macrophages were pre-differentiated with IL-4 to boost TREM2 expression and lipid accumulation (mimicking foamy macrophages in the alveolar pneumonia) or kept as unpolarized controls. We then infected both groups with a fluorescent *M.tb* reporter strain that expresses GFP preferentially in live (actively respiring) bacteria and mCherry constitutively (*53, 54*). After 24 hours, confocal microscopy revealed that macrophages with high TREM2 and lipid content harbored approximately twice as many viable (GFP$^+$) bacilli per cell compared to control macrophages (**Figure 4E, F**, **Supplemental Figure 18B**). In other words, *M.tb* survival was significantly higher inside foamy TREM2$^+$ macrophages. This result was consistent across multiple donors. We quantified the GFP/mCherry fluorescence ratio and observed a clear skew toward GFP (indicating live bacilli) in the TREM2$^+$/foamy macrophage condition.

We next asked whether immunometabolic reprogramming of the TREM2$^+$ macrophages would enhance their bactericidal activity. Given the known connection between vitamin D and macrophage antimicrobial responses in TB(*34*), and reports that 1,25-dihydroxyvitamin D_3 (the active form of vitamin D) can drive *CAMP* (cathelicidin) expression, we tested vitamin D_3

treatment on our macrophages. Remarkably, vitamin D_3 pretreatment significantly downregulated TREM2 on macrophages (by flow cytometry) (**Supplemental Figure 19A, B**). When these vitamin D–treated macrophages were infected with *M.tb* (dual GFP/mCherry reporter), we observed a marked reduction in GFP signal per bacterium, indicating fewer live bacilli, in both $1,25(OH)_2D_3$-treated $TREM2^+$ macrophages and MDMs (**Figure 4G**). By CFU assay, vitamin D_3 treatment led to ~1 $\log_{10}$ lower bacterial burden by 4 days post-infection in both $TREM2^+$ macrophages and unsorted macrophages ($p < 0.0001$) (**Figure 4H**). These findings suggest that vitamin D's immunomodulatory effects include suppressing the $TREM2^+$ foamy macrophage phenotype and/or enhancing antimicrobial pathways. This aligns with clinical observations that vitamin D supplementation can modestly enhance TB treatment outcomes, presumably by boosting macrophage killing mechanisms (e.g., cathelicidin production) (*55-58*).

In summary, our functional experiments demonstrate that the $TREM2^+$ foamy macrophage state directly contributes to *M.tb* survival. *M.tb*'s own lipids increase *M.tb* survival in macrophages; an intervention that counters this (such as vitamin D) restore macrophage ability to suppress the bacteria. Together with the spatial data, these results paint a coherent picture: in early TB infection, *M.tb* co-opts macrophages in the alveolar pneumonia to become foamy lipid-loaded cells (via TREM2 and other pathways), which then serve as incubators for the bacteria, all while mounting a muted immune response. This foamy macrophage stage likely persists until either the host's adaptive immune response catches up, forming organized granulomas to contain the infection, or until tissue damage leads to cavitation and transmission of the bacilli to new hosts.

Discussion

This study reframes the early cellular events in human TB, demonstrating that a foamy alveolar pneumonia precedes and is distinct from organized granulomas, and that this lesion defines a critical spatial niche for *M.tb* (*10, 16, 59*). We found that these alveolar lesions, dominated by TREM2^{+} lipid-laden macrophages, contained abundant *M.tb* antigen and transcripts but lacked detectable acid-fast bacilli and were sputum culture negative, consistent with the AFB-negative clinical presentation that prompted surgical biopsy for diagnosis. This highlights that even in the absence of readily culturable organisms, the alveolar pneumonia harbors bacillary material at the air, lung interface, a finding consistent with growing evidence that subclinical TB contributes substantially to transmission (*1, 3, 10, 16, 59*).

Epidemiological surveys now suggest that more than half of pulmonary TB cases in endemic areas are asymptomatic at the time of detection, yet harbor viable bacilli and can spread infection (*1*). Transmission can occur even without coughing, as normal tidal breathing generates aerosols that carry bacilli from the alveoli (*2*). Our findings provide a cellular correlate to this phenomenon: alveolar lesions enriched for TREM2^{+} foamy macrophages and bacillary antigens are strategically positioned to serve as an early launching pad for contagious TB. In contrast, granuloma cores within the same lungs were enriched for antimicrobial pathways and surrounded by lymphocytes and other cell types, representing an immune containment strategy that develops only later in disease progression. This compartmentalization, permissive pneumonia versus bactericidal or bacteriostatic granulomas, helps explain how *M.tb* can persist and spread before overt clinical disease is recognized.

The patients studied here had negative sputum smears and cultures, yet their lung biopsies demonstrated *M.tb* DNA by Xpert, mRNA transcripts, and mycobacterial antigens, findings most consistent with active pulmonary TB. WHO guidelines recommend nucleic acid amplification tests (NAATs) such as Xpert on biopsy specimens when conventional microbiology is negative (*60*). The diagnostic weight of mRNA is particularly strong, as transcripts are highly

labile (genome-wide half-life ~9.5 minutes in vitro) and clear rapidly once bacilli lose viability (*61, 62*); clinical studies show mRNA disappears early during therapy, before DNA levels fall (*63*). Antigen detection in tissue, even when AFB stains are negative, further supports the presence of metabolically active organisms (*43*). Recent longitudinal cohorts demonstrate that many symptomatic, culture-negative individuals harbor *M.tb* biomarkers, including mRNA transcripts and growth in augmented cultures, despite negative standard cultures (*64*).

Our spatial transcriptomic and single-cell analyses demonstrated that alveolar pneumonia regions are enriched for lipid metabolism and scavenger receptor programs, whereas granuloma cores show robust induction of antimicrobial pathways. Using a curated antimicrobial gene panel, we confirmed that transcripts encoding key antimicrobial proteins, such as cathelicidin and granulysin, were abundant in macrophages in granulomas and T cells but nearly absent from macrophages in the alveolar pneumonia. Thus, in the very microanatomic locations with the highest antigen and RNA burden, the antimicrobial immune machinery was largely silent. This transcriptional observation was complemented by functional assays: in vitro, macrophages enriched in the TREM2^{+} foamy phenotype harbored approximately twice as many viable bacilli as unpolarized controls. Together, the evidence suggest that TREM2^{+} macrophages form a permissive niche that enable persistence and transmission of *M.tb*.

A major mechanistic advance is the identification of TREM2^{+} macrophages as the molecularly defined foamy cell population in early TB pneumonia (*17, 18*). These cells share a conserved immunometabolic program with TREM2^{+} lipid-associated macrophages found in atherosclerosis and neurodegenerative disease, expressing genes such as APOE, PLIN2, and CD163 (*12, 20*). In the context of TB, however, their phenotype shifts from tissue-restorative to pathogen-permissive, characterized by diminished antimicrobial peptide expression, elevated IL-10, and a muted pro-inflammatory profile (*21, 23, 39*). Mechanistically, our data demonstrate that mycobacterial virulence lipids, especially phthiocerol dimycocerosate (PDIM) and free

mycolic acids, potently induce TREM2 expression and lipid droplet accumulation in human macrophages, surpassing even live *M.tb* infection in their capacity to skew cells into a foamy state. These findings extend prior work showing that non-glycosylated mycolic acids engage TREM2 (*22, 23*), by establishing PDIM as an additional, potent activator of this pathway. PDIM, already recognized as a critical virulence factor for intracellular survival, is able to disseminate into host membranes, suppress phagocytic clearance, and activate TREM2–DAP12 signaling, underscoring its multifaceted role in immune evasion (*41, 42, 52, 65-67*). In vivo, this lipid-driven skewing likely contributes to the predominance of TREM2$^+$ macrophages in pneumonia lesions and their role as antigen- and RNA-rich reservoirs.

Our in vitro findings also highlight the possibility of intervening to counteract this pathogenic reprogramming. We demonstrated that treatment of human macrophages with 1,25-dihydroxyvitamin D_3 downregulated TREM2 expression, reduced lipid droplet accumulation, and restored bactericidal activity. Vitamin D treated macrophages showed a ten-fold reduction in viable bacilli compared to untreated cells. These results provide a mechanistic link to prior observations that vitamin D enhances macrophage antimicrobial responses and support further exploration as a host-directed therapy in early TB (*34, 55, 56*). More broadly, they suggest that immunometabolic interventions, either boosting protective antimicrobial mechanisms like vitamin D or inhibiting pathogen-exploited pathways like TREM2, could re-educate foamy macrophages within the alveolar pneumonia and limit bacterial growth.

In summary, our study proposes a new interpretation of TB pathogenesis that identifies foamy alveolar pneumonia as a critical target for early intervention to prevent progression and transmission. This lesion, dominated by TREM2$^+$ lipid-associated macrophages, is characterized by abundant antigen and transcripts, impaired antimicrobial responses, and a location poised for transmission. Targeting this niche, through early detection and appropriate therapy may provide a pivotal opportunity to prevent disease progression and limit transmission in symptomatic and asymptomatic infections.

References

1. J. C. Emery *et al.*, Estimating the contribution of subclinical tuberculosis disease to transmission: An individual patient data analysis from prevalence surveys. *eLife* **12**, (2023).
2. R. Dinkele *et al.*, Aerosolization of Mycobacterium tuberculosis by Tidal Breathing. *Am. J. Respir. Crit. Care Med.* **206**, 206-216 (2022).
3. B. R. Bloom, A half-century of research on tuberculosis: Successes and challenges. *J. Exp. Med.* **220**, (2023).
4. F. de Le Boe Sylvius, *Francisci Deleboe, Sylvii Opera medica*. (Apud D. Elsevirium et A. Wolfgang, 1679).
5. R. T. H. Laennec, A treatise on the diseases of the chest: in which they are described according to their anatomical characters, and their diagnosis established on a new principle by means of acoustick instruments. *(No Title)*, (1821).
6. E. M. Medlar, The behavior of pulmonary tuberculous lesions; a pathological study. *Am Rev Tuberc* **71**, 1-244 (1955).
7. A. E. Pitchenik *et al.*, Opportunistic infections and Kaposi's sarcoma among Haitians: evidence of a new acquired immunodeficiency state. *Ann. Intern. Med.* **98**, 277-284 (1983).
8. J. Keane *et al.*, Tuberculosis associated with infliximab, a tumor necrosis factor alpha-neutralizing agent. *N. Engl. J. Med.* **345**, 1098-1104 (2001).
9. D. G. Russell, P. J. Cardona, M. J. Kim, S. Allain, F. Altare, Foamy macrophages and the progression of the human tuberculosis granuloma. *Nat Immunol* **10**, 943-948 (2009).
10. G. Canetti, *The Tubercle Bacillus in the Pulmonary Lesion of Man: Histobacteriology and Its Bearing on the Therapy of Pulmonary Tuberculosis*. (Springer Publishing Company, 1955).
11. R. L. Hunter, Tuberculosis as a three-act play: A new paradigm for the pathogenesis of pulmonary tuberculosis. *Tuberculosis (Edinburgh, Scotland)* **97**, 8-17 (2016).
12. M. Bedard *et al.*, A terpene nucleoside from M. tuberculosis induces lysosomal lipid storage in foamy macrophages. *J. Clin. Invest.* **133**, (2023).
13. P. Peyron *et al.*, Foamy macrophages from tuberculous patients' granulomas constitute a nutrient-rich reservoir for M. tuberculosis persistence. *PLoS Pathog.* **4**, e1000204 (2008).
14. J. L. Flynn, J. Chan, Immunology of tuberculosis. *Annu. Rev. Immunol.* **19**, 93-129 (2001).
15. C. E. Barry, III *et al.*, The spectrum of latent tuberculosis: rethinking the biology and intervention strategies. *Nat Rev Microbiol* **7**, 845-855 (2009).
16. R. L. Hunter, C. Jagannath, J. K. Actor, Pathology of postprimary tuberculosis in humans and mice: contradiction of long-held beliefs. *Tuberculosis (Edinb)* **87**, 267-278 (2007).
17. D. A. Jaitin *et al.*, Lipid-Associated Macrophages Control Metabolic Homeostasis in a Trem2-Dependent Manner. *Cell* **178**, 686-698 e614 (2019).
18. M. T. Patterson *et al.*, Trem2 promotes foamy macrophage lipid uptake and survival in atherosclerosis. *Nature cardiovascular research* **2**, 1015-1031 (2023).
19. A. Ruiz *et al.*, Assessing the role of the TREM2 p. R47H variant as a risk factor for Alzheimer's disease and frontotemporal dementia. *Neurobiol. Aging* **35**, 444. e441-444. e444 (2014).
20. S. Krasemann *et al.*, The TREM2-APOE Pathway Drives the Transcriptional Phenotype of Dysfunctional Microglia in Neurodegenerative Diseases. *Immunity* **47**, 566-581 e569 (2017).
21. D. L. Kober, T. J. Brett, TREM2-Ligand Interactions in Health and Disease. *J. Mol. Biol.* **429**, 1607-1629 (2017).

22. E. Iizasa *et al.*, TREM2 is a receptor for non-glycosylated mycolic acids of mycobacteria that limits anti-mycobacterial macrophage activation. *Nature communications* **12**, 2299 (2021).
23. A. Dabla *et al.*, TREM2 Promotes Immune Evasion by Mycobacterium tuberculosis in Human Macrophages. *mBio* **13**, e0145622 (2022).
24. W. N. van der *et al.*, M. tuberculosis and M. leprae translocate from the phagolysosome to the cytosol in myeloid cells. *Cell* **129**, 1287-1298 (2007).
25. J. Bustamante *et al.*, Germline CYBB mutations that selectively affect macrophages in kindreds with X-linked predisposition to tuberculous mycobacterial disease. *Nat Immunol* **12**, 213-221 (2011).
26. E. F. McCaffrey *et al.*, The immunoregulatory landscape of human tuberculosis granulomas. *Nat. Immunol.* **23**, 318-329 (2022).
27. P. F. Barnes *et al.*, Compartmentalization of a CD4+ T lymphocyte subpopulation in tuberculous pleuritis. *J. Immunol.* **142**, 1114-1119 (1989).
28. M. S. Inkeles *et al.*, Comparison of molecular signatures from multiple skin diseases identifies mechanisms of immunopathogenesis. *J. Invest. Dermatol.* **135**, 151-159 (2015).
29. M. S. Inkeles *et al.*, Cell-type deconvolution with immune pathways identifies gene networks of host defense and immunopathology in leprosy. *JCI insight* **1**, e88843 (2016).
30. K. J. Travaglini *et al.*, A molecular cell atlas of the human lung from single-cell RNA sequencing. *Nature* **587**, 619-625 (2020).
31. F. Ma *et al.*, The cellular architecture of the antimicrobial response network in human leprosy granulomas. *Nat. Immunol.* **22**, 839-850 (2021).
32. G. Wang, X. Li, Z. Wang, APD3: the antimicrobial peptide database as a tool for research and education. *Nucleic Acids Res.* **44**, D1087-1093 (2016).
33. P. R. Andrade *et al.*, Dynamics of Th1/Th17 responses and antimicrobial pathways in leprosy skin lesions. *J. Clin. Invest.*, (2025).
34. P. T. Liu *et al.*, Toll-like receptor triggering of a vitamin D-mediated human antimicrobial response. *Science* **311**, 1770-1773 (2006).
35. S. Stenger *et al.*, An antimicrobial activity of cytolytic T cells mediated by granulysin. *Science* **282**, 121-125 (1998).
36. S. J. Balin *et al.*, Human antimicrobial cytotoxic T lymphocytes, defined by NK receptors and antimicrobial proteins, kill intracellular bacteria. *Sci Immunol* **3**, 10.1126/sciimmunol.aat7668 (2018).
37. A. T. Dang *et al.*, IL-26 contributes to host defense against intracellular bacteria. *J. Clin. Invest.* **129**, 1926-1939 (2019).
38. S. Realegeno *et al.*, S100A12 Is Part of the Antimicrobial Network against Mycobacterium leprae in Human Macrophages. *PLoS Pathog.* **12**, e1005705 (2016).
39. X. Shang *et al.*, Triggering Receptor Expressed on Myeloid Cells 2 Mediates the Involvement of M2-Type Macrophages in Pulmonary Tuberculosis Infection. *Journal of inflammation research* **17**, 1919-1928 (2024).
40. L. A. Ramon-Luing, Y. Palacios, A. Ruiz, N. A. Tellez-Navarrete, L. Chavez-Galan, Virulence Factors of Mycobacterium tuberculosis as Modulators of Cell Death Mechanisms. *Pathogens* **12**, (2023).
41. C. V. Mulholland *et al.*, Propionate prevents loss of the PDIM virulence lipid in Mycobacterium tuberculosis. *Nature microbiology* **9**, 1607-1618 (2024).
42. J. Augenstreich *et al.*, Phthiocerol Dimycocerosates From Mycobacterium tuberculosis Increase the Membrane Activity of Bacterial Effectors and Host Receptors. *Frontiers in cellular and infection microbiology* **10**, 420 (2020).

43. K. Nargan *et al.*, Spatial distribution of Mycobacterium tuberculosis mRNA and secreted antigens in acid-fast negative human antemortem and resected tissue. *EBioMedicine* **105**, 105196 (2024).
44. Y. Wang *et al.*, TREM2 lipid sensing sustains the microglial response in an Alzheimer's disease model. *Cell* **160**, 1061-1071 (2015).
45. F. L. Yeh, Y. Wang, I. Tom, L. C. Gonzalez, M. Sheng, TREM2 Binds to Apolipoproteins, Including APOE and CLU/APOJ, and Thereby Facilitates Uptake of Amyloid-Beta by Microglia. *Neuron* **91**, 328-340 (2016).
46. M. Colonna, Y. Wang, TREM2 in neurodegenerative diseases. *Nature Reviews Immunology* **23**, 15-29 (2023).
47. I. R. Turnbull *et al.*, Cutting edge: TREM-2 attenuates macrophage activation. *J. Immunol.* **177**, 3520-3524 (2006).
48. S. Gordon, F. O. Martinez, Alternative activation of macrophages: mechanism and functions. *Immunity* **32**, 593-604 (2010).
49. M. Knight, J. Braverman, K. Asfaha, K. Gronert, S. Stanley, Lipid droplet formation in Mycobacterium tuberculosis infected macrophages requires IFN-gamma/HIF-1alpha signaling and supports host defense. *PLoS Pathog.* **14**, e1006874 (2018).
50. K. A. McDonough, Y. Kress, B. R. Bloom, Pathogenesis of tuberculosis: Interaction of Mycobacterium tuberculosis with macrophages. *Infect Immun* **61**, 2763-2773 (1993).
51. R. Teitelbaum *et al.*, Mycobacterial infection of macrophages results in membrane-permeable phagosomes. *Proc. Natl. Acad. Sci. U. S. A.* **96**, 15190-15195 (1999).
52. J. Quigley *et al.*, The Cell Wall Lipid PDIM Contributes to Phagosomal Escape and Host Cell Exit of Mycobacterium tuberculosis. *mBio* **8**, (2017).
53. C. J. Martin *et al.*, Efferocytosis is an innate antibacterial mechanism. *Cell Host Microbe* **12**, 289-300 (2012).
54. M. Ouimet *et al.*, Mycobacterium tuberculosis induces the miR-33 locus to reprogram autophagy and host lipid metabolism. *Nat. Immunol.* **17**, 677-686 (2016).
55. A. R. Martineau *et al.*, High-dose vitamin D(3) during intensive-phase antimicrobial treatment of pulmonary tuberculosis: a double-blind randomised controlled trial. *Lancet* **377**, 242-250 (2011).
56. D. Ganmaa *et al.*, Vitamin D, tuberculin skin test conversion, and latent tuberculosis in Mongolian school-age children: a randomized, double-blind, placebo-controlled feasibility trial. *Am. J. Clin. Nutr.* **96**, 391-396 (2012).
57. H. X. Wu *et al.*, Effects of vitamin D supplementation on the outcomes of patients with pulmonary tuberculosis: a systematic review and meta-analysis. *BMC Pulm. Med.* **18**, 108 (2018).
58. G. Patti *et al.*, Potential Role of Vitamins A, B, C, D and E in TB Treatment and Prevention: A Narrative Review. *Antibiotics (Basel, Switzerland)* **10**, (2021).
59. G. Wells *et al.*, Micro-Computed Tomography Analysis of the Human Tuberculous Lung Reveals Remarkable Heterogeneity in Three-dimensional Granuloma Morphology. *Am. J. Respir. Crit. Care Med.* **204**, 583-595 (2021).
60. O. World Health, "WHO consolidated guidelines on tuberculosis, 2023–2024 update," (World Health Organization, Geneva, Switzerland, 2023).
61. T. R. Rustad *et al.*, Global analysis of mRNA stability in Mycobacterium tuberculosis. *Nucleic Acids Res.* **41**, 509-517 (2013).
62. D. A. Vargas-Blanco, et al., Mycobacterium tuberculosis Persists in Acidic Environments for Decades by Maintaining Translation. *mBio* **10**, e00957-00919 (2019).
63. T. J. Hellyer, et al., Rapid disappearance of Mycobacterium tuberculosis RNA from sputum after initiation of successful chemotherapy. *J. Clin. Microbiol.* **37**, 518-523 (1999).

64. Y. L. Xie *et al.*, Prominence of Mycobacterium tuberculosis biomarkers among sputum culture-negative clinic attendees, independent of Ultra status. *Journal of infection and public health* **18**, 102791 (2025).
65. C. J. Cambier *et al.*, Mycobacteria manipulate macrophage recruitment through coordinated use of membrane lipids. *Nature* **505**, 218-222 (2014).
66. E. Mittal *et al.*, Mycobacterium tuberculosis virulence lipid PDIM inhibits autophagy in mice. *Nature microbiology* **9**, 2970-2984 (2024).
67. A. Schami *et al.*, Drug resistant Mycobacterium tuberculosis strains have altered cell envelope hydrophobicity that influences infection outcomes in human macrophages. *Sci. Rep.* **14**, 30840 (2024).

Acknowledgments

We thank Dr. Robert Hunter for providing insight and advice on the lung pathology of tuberculosis (TB) as well as the pathogenesis of TB infection. We are grateful to Christopher C. Tai K. for assistance with single-cell RNA sequencing (scRNA-seq) from FFPE pulmonary TB samples, and to Annaliza Legaspi for help with blood donor selection and processing. We acknowledge the University of California–Los Angeles California NanoSystems Institute Advanced Light Microscopy Core Facility for assistance with confocal studies (RRID: SCR_022789). We thank Barbara Dillon from the UCLA High Containment Facilities for support with BSL-3–required assays. We also thank the UCLA Technology Center for Genomics & Bioinformatics (TCGB) for assistance with GeoMX and scRNA-seq, the Translational Pathology Core Laboratory (TPCL) for sectioning FFPE TB samples for CosMx and scRNA-seq, and the UCLA Jonsson Comprehensive Cancer Center (JCCC) Flow Cytometry Core Facility for support with flow cytometry assays.

Funding

The funding sources for this work were: NIH grants R01 AI022553, R01 AR040312, R01 AI166313, R01 AI169526, P50 AR080594, U01DK134321, R01DK135620 and U19AI181102.

Authors contribution

R.L.M. supervised and conceptualized the study. R.M.B.T. led the experimental work, including functional assays and CosMx, and contributed to conceptualization. C.B. contributed to sample collection, conceptualization and writing. J.P. analyzed GeoMX data and contributed to bioinformatics. C.W. analyzed FFPE RNA-seq data. J.W. contributed to CosMx, scRNA-seq, and functional analysis. B.J.A.S. performed M. tuberculosis infections and CFU assays. P.R.A. conducted RNAscope analysis. L.M., K.L., and F.M. performed bioinformatics and gene signature analyses. P.D. supported CosMx assays. L.F. contributed to mycobacterial ligand

assays. K.M. and A.P. performed immunohistochemistry. S.M.F., M.R.B., E.R., and S.R. provided pathology support. A.J.C.S. supported RNAscope assays. E.K., M.C., S.B., and D.L.B. supported gene signature analyses. P.S.B., B.D.B., M.P., and J.T.B. contributed to data interpretation and manuscript revision. B.R.B. contributed to conceptualization, data interpretation and writing. The manuscript was written by R.M.B.T., B.R.B. and R.L.M.

Competing interests

"Authors declare that they have no competing interests."

Data and Code Availability

GeoMx transcriptomic data have been deposited in the Gene Expression Omnibus GEO) under accession number GSE301876. The FFPE scRNA-seq data generated in this study have been deposited in the GEO under accession number GSE301610, including sample series GSM9086459. All data supporting the findings of this study are also available at Zenodo (DOI: 10.5281/zenodo.15750734). Custom scripts and analysis pipelines are available on GitHub at https://github.com/modlab246/TREM2_PTB.

Supplementary Materials

Materials and Methods

Figs. S1 to S19

Tables S1 to S10

References (8)

Figure 1

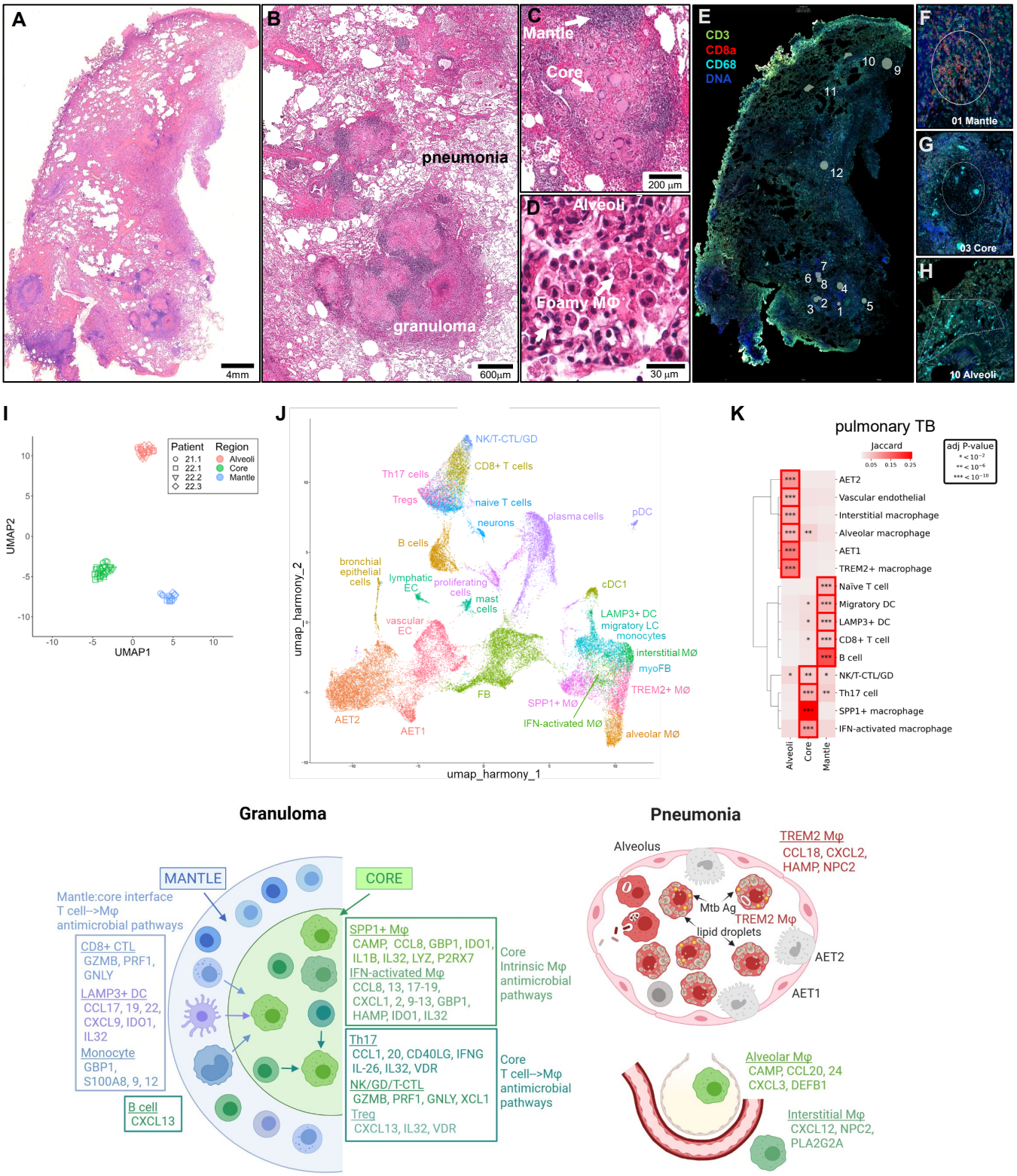

Figure 1. GeoMx spatial profiling of the human transcriptome in pulmonary TB (PTB). (A-B) Pulmonary TB biopsy specimen from PTB 21.1a, H&E. (C) Organized granuloma, H&E, (D) Pneumonitis showing alveoli with foamy macrophages, (E) Regions of interest (ROI), serial section, immunofluorescence, (F) Mantle- ROI 01, (G) Core- ROI 03, (H) Alveoli- ROI 10, (I) UMAP representation of all ROIs. (J) UMAP representation of PTB cell signature identified by scRNA-seq. (K) Jaccard overlap of the GeoMx spatial profiling data with the PTB scRNA-seq data. (L) Distribution of antimicrobial genes in PTB identified by integrating the GeoMx spatial profiling data with the scRNA-seq data.

Figure 2

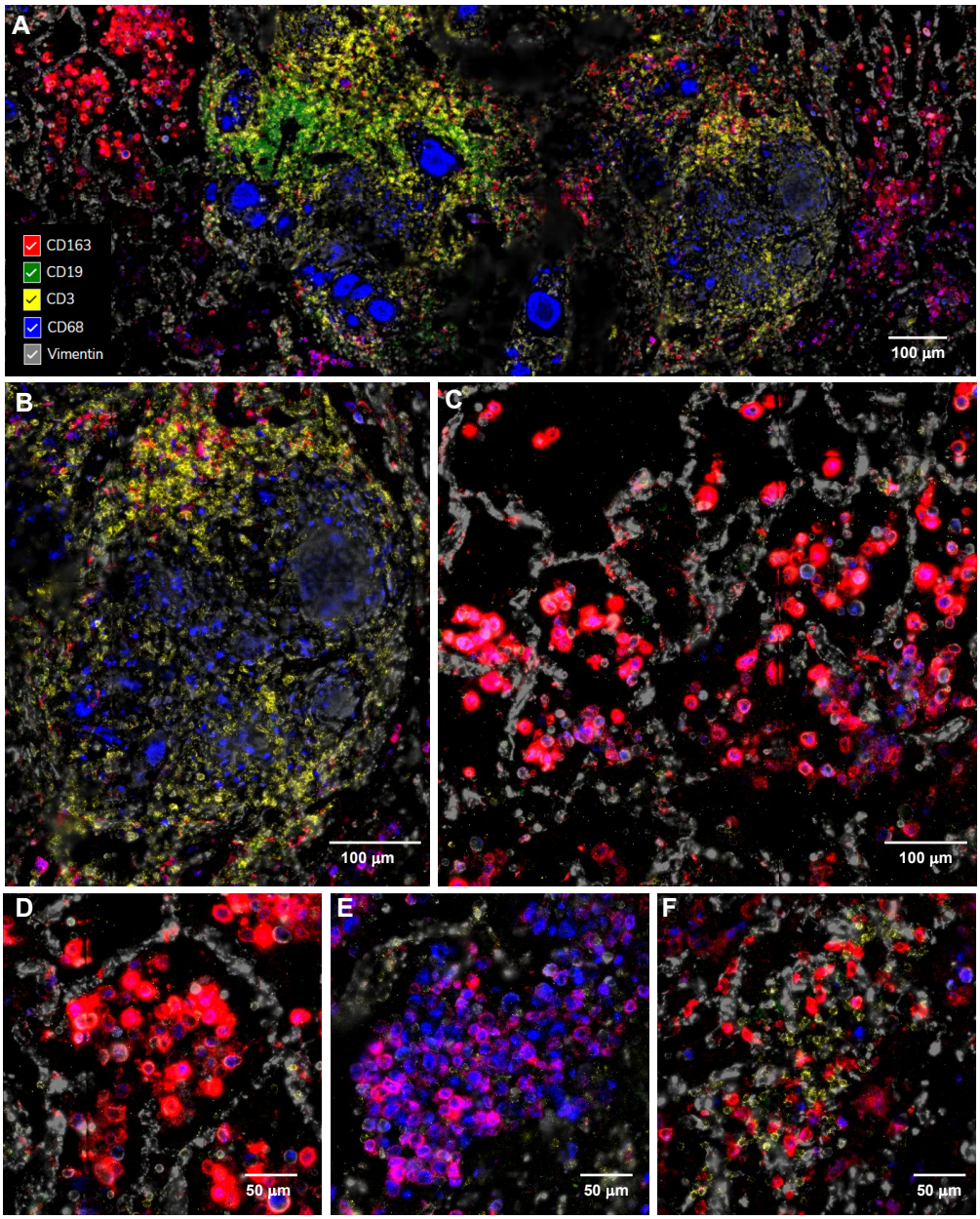

Figure 2. Immunofluorescence images obtained using the CosMx spatial profiling with the human protein panel, illustrating the spatial expression of immune cell markers in active pulmonary tuberculosis (TB). (A) Overview of immune cell distribution within the active pulmonary TB lesion. The granuloma core contains CD68^{+} macrophages (blue) and CD3^{+} T cells (yellow). The granuloma mantle contains CD3^{+} T cells (yellow) and CD19^{+} B cells (green). The alveoli contain prominent CD163^{+} macrophages (red), some with CD68 expression (blue). Vimentin (gray) is present on many cells in the lesions but particularly highlights the alveolar structure by staining alveolar epithelial cells. (B) Localization of immune cells within granulomas. (C–F) Distribution of immune cells in alveolar regions showing heterogeneity of macrophage phenotype and variability in the presence or absence of T cells. Scale bars: 100 µm (low magnification) and 50 µm (high magnification).

Figure 3

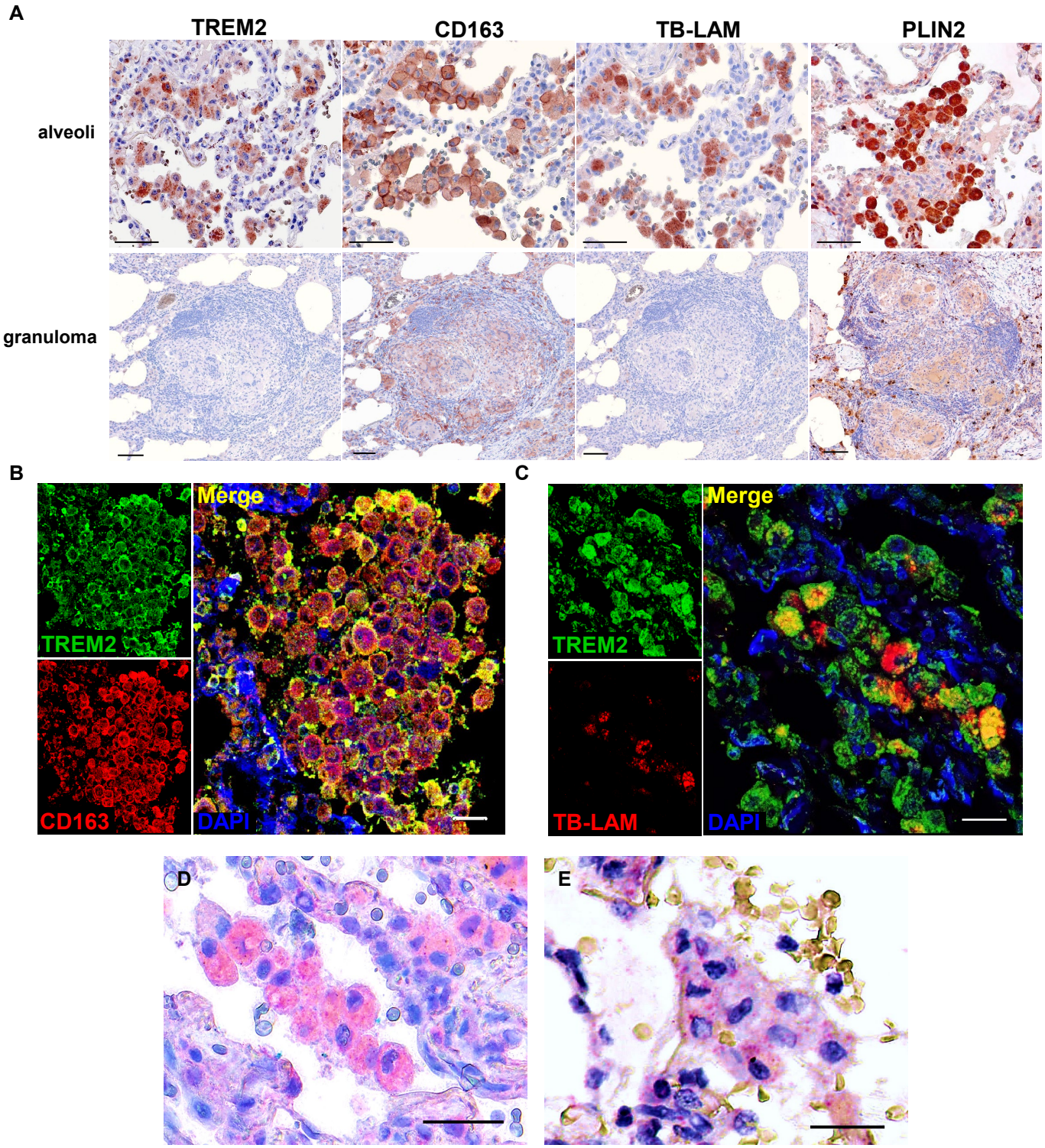

Figure 3: Immunohistochemical analysis of the alveolar pneumonia in pulmonary tuberculosis (PTB) tissue shows that (A) TREM2-associated macrophage signature markers, TREM2, CD163 and PLIN2, as well as Mycobacterium tuberculosis (*Mtb*) lipoarabinomannan (LAM) are enriched in areas of alveolar pneumonia compared to the granulomas, (B) TREM2 is co-expressed with CD163, (C) *Mtb* LAM colocalizes with TREM2^{+} macrophages, (D) *Mtb* proteins (red staining) accumulate within foamy macrophages within alveoli, counterstain hematoxylin, and (E) *Mtb* RNA is observed as red puncta present in foamy macrophages within alveoli by in situ hybridization (RNAscope), counterstained with hematoxylin. The brown staining cells represent erythrocytes. All representative images are shown from four independent PTB specimens (scale bars: 40 μm for A; 20 μm for B–E).

Figure 4

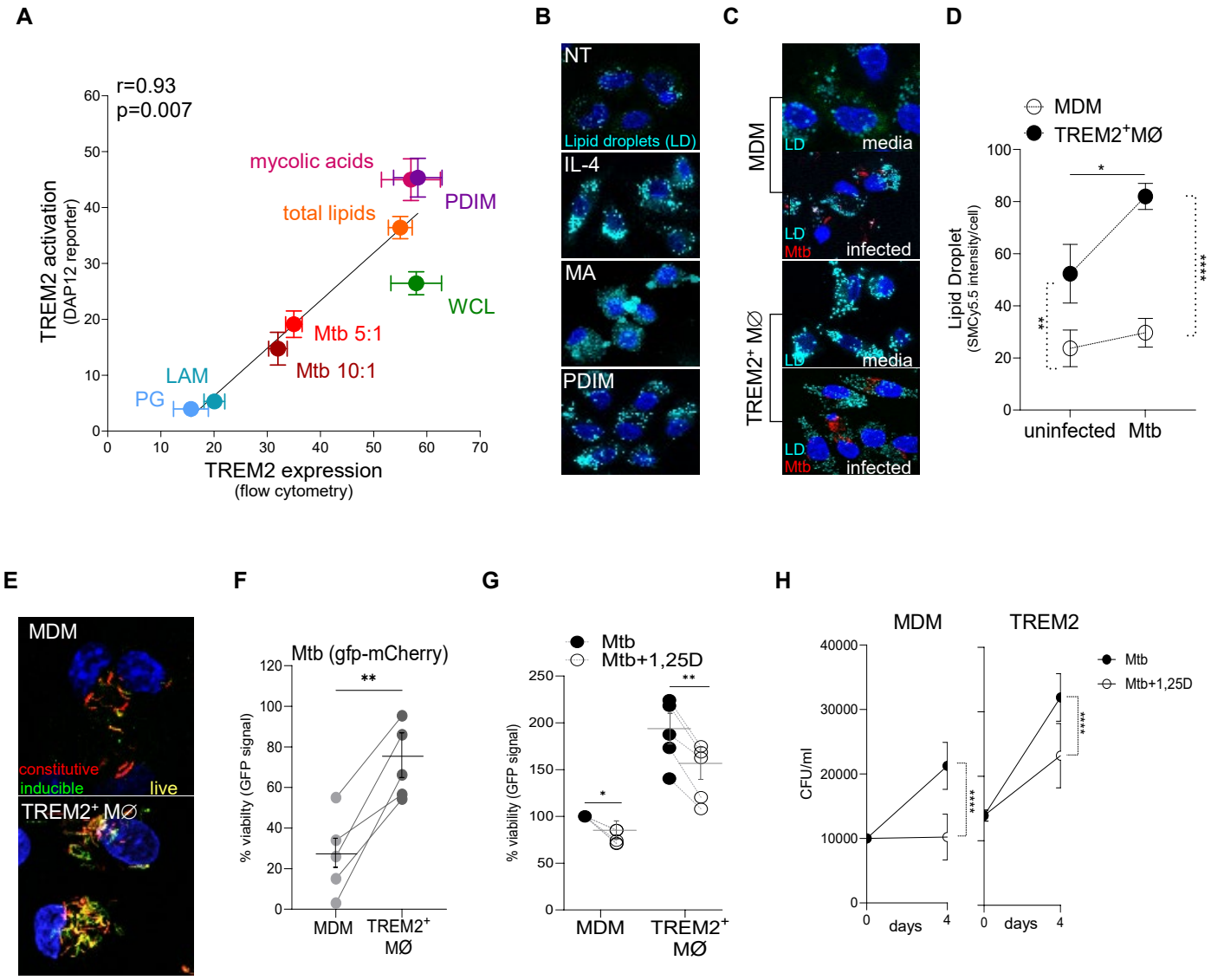

Figure 4. TREM2⁺ macrophage (M∅) interactions with *M. tuberculosis* (*Mtb*). (A) TREM2 activation correlates with its upregulation in monocyte-derived macrophages (MDMs) stimulated with *Mtb*-associated ligands (n = 7). (B) Mycolic acids (MA) and phthiocerol dimycocerosates (PDIM) induce lipid droplet (LD) aggregation at levels comparable to IL-4-polarized TREM2⁺ M∅. (C–D) TREM2⁺ M∅ exhibit a higher accumulation of lipid droplets than MDMs in uninfected and *Mtb*-infected conditions (n = 5). Lipid droplets (LD) were labeled with SMCy5.5 (cyan). (E–F) *Mtb* preferentially proliferates in TREM2⁺ M∅ compared to MDMs. M∅ were infected with *Mtb* (GFP-mCherry), with inducible GFP and constitutive mCherry expression (n = 5). (G) M∅ were stimulated with 1,25(OH)2D3 and infected with *Mtb* (GFP-mCherry) (n = 5). Images were acquired using confocal microscopy, with DAPI used to stain nuclei. Images were acquired using confocal microscopy, with DAPI used to stain nuclei. Quantification was performed using ImageJ. (H) Antimicrobial activity of MDM and TREM2⁺ M∅ following 1,25(OH)2D3 stimulation. Cells were stimulated with 1,25(OH)2D3 and infected with *Mtb*. The number of viable *Mtb* bacteria was assessed by CFU assay (n=5). (A, D and F) One-way ANOVA with Tukey multi-comparison test, (G-H) Two-way ANOVA with Fisher multi-comparison test. (B, C, and E) Fluorescent images are representative of 5 individual donors. Statistical significance: * $p \leq 0.05$, ** $p \leq 0.01$, ***$p \leq 0.001$, ****$p \leq 0.0001$.